Ab Initio Calculations of the Main Crystal Surfaces of Forsterite (Mg2SiO4): A Preliminary Study to Understand the Nature of Geochemical Processes at the Olivine Interface

ARTICLE *in* THE JOURNAL OF PHYSICAL CHEMISTRY C · JANUARY 2014

Impact Factor: 4.77 · DOI: 10.1021/jp409837d

6 AUTHORS, INCLUDING:

Mauro Prencipe
Università degli Studi di Torino
74 PUBLICATIONS **1,121** CITATIONS
SEE PROFILE

Raffaella Demichelis
Curtin University
35 PUBLICATIONS **555** CITATIONS
SEE PROFILE

Marco De La Pierre
Curtin University
28 PUBLICATIONS **265** CITATIONS
SEE PROFILE

Fabrizio Nestola
University of Padova
285 PUBLICATIONS **1,844** CITATIONS
SEE PROFILE

THE JOURNAL OF PHYSICAL CHEMISTRY C

Article

pubs.acs.org/JPCC

Ab Initio Calculations of the Main Crystal Surfaces of Forsterite (Mg_2SiO_4): A Preliminary Study to Understand the Nature of Geochemical Processes at the Olivine Interface

M. Bruno,*[,†] F. R. Massaro,[‡] M. Prencipe,[†] R. Demichelis,[§] M. De La Pierre,[∥] and F. Nestola[‡]

[†]Dipartimento di Scienze della Terra, Università degli Studi di Torino, Via Valperga Caluso 35, 10125 Torino, Italy

[‡]Dipartimento di Geoscienze, Università degli Studi di Padova, Via Gradenigo 6, 35131 Padova, Italy

[§]Nanochemistry Research Institute, Department of Chemistry, Curtin University, P.O. Box U1987, Perth, WA 6845, Australia

[∥]Dipartimento di Chimica, Università degli Studi di Torino and NIS -Nanostructured Interfaces and Surfaces - Centre of Excellence, Via P. Giuria 7, 10125 Torino, Italy

Supporting Information

ABSTRACT: We present an accurate ab initio study of the structure and surface energy at 0 K of the (010), (101), (111), (001), (110), (120), and (021) faces of forsterite (Mg_2SiO_4) using the hybrid Hartree−Fock/density functional B3LYP Hamiltonian and a localized all-electron Gaussian-type basis set. According to the surface energy values, the stability order of the forsterite faces was found to be (010) < (120) < (001) < (101) < (111) < (021) < (110). Then, the equilibrium shape of forsterite was drawn and compared with the previous ones obtained at an empirical level. Our results were combined with experimental evidence to develop some considerations about the shape and genesis of olivine included in diamond. They provide crucial information on the diamond formation mechanism with respect to its guest inclusions, a topic that is still under strong debate in the scientific community. In particular, we discuss the peculiar crystal morphology of olivine included in diamond, and we demonstrate that it cannot be considered as evidence of syngenesis (i.e., inclusion and host diamond formed at the same time). Furthermore, if the morphology of olivine is modified during its encapsulation in diamond but it does not show a preferential orientation with respect to diamond, we can state that (i) the bulk of olivine is protogenetic (i.e., a piece of previously formed olivine is encapsulated by the host diamond), whereas (ii) its shape is syngenetic, that is, the morphology is rearranged during the encapsulation.

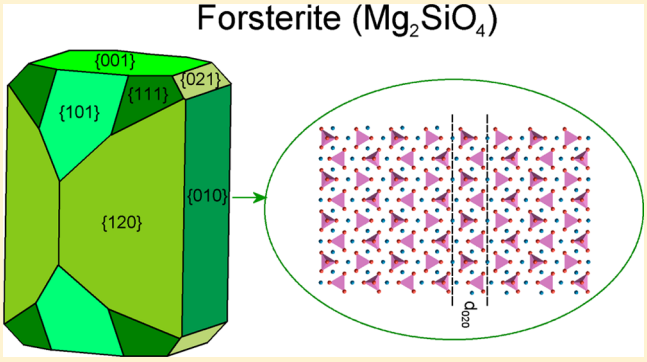

1. INTRODUCTION

Olivine exists as a complete isomorphous series, with composition ranging from forsterite (Mg_2SiO_4) to fayalite (Fe_2SiO_4), but the most common olivines are richer in magnesium than in iron.[1] Other than being one of the major components of the Earth's mantle and of many meteorite classes, it is often detected on the surface of extraterrestrial planetary bodies and, more generally, in the spectra of astronomical targets.[2] As a consequence, olivine plays a fundamental role in defining the properties, influencing the physicochemical processes, and recording the history of both terrestrial and extraterrestrial environments.[3−6]

Within the wide family of natural phenomena that involve olivine, of particular interest are those occurring at the interface between olivine and other materials, such as minerals and water environments. For example, the olivine/water interface is increasingly raising the attention of the whole international scientific community because of the natural and widespread occurrence of reactions that can lead to (i) carbon dioxide storage, (ii) the production of hydrogen and synthesis of organic molecules, and (iii) the formation of serpentines (lizardite, antigorite, chrysotile).[7−10]

An important process in which the olivine/mineral interface plays a fundamental role is relative to the inclusions of olivine in diamond (DIs). Such inclusions, together with other silicates, oxide, and sulfides found in diamonds, are among the deepest materials originating from Earth's interior reaching the planet's surface. Diamonds are billions of years old and remain unaltered over time, preserving the pristine conditions of Earth. Therefore, their study plays a key role in understanding and interpreting the geodynamics, geophysics, petrology, geochemistry, and mineralogy of Earth's mantle from the lithosphere to the lowermost part (see Stachel and Harris[11] and references therein).

A comprehensive knowledge of olivine surface energetics and morphology at the atomic level is of extreme importance to

Received: October 3, 2013
Revised: January 12, 2014
Published: January 13, 2014

understand the true nature of these processes and, more generally, all processes involving the olivine interface. However, to the authors' knowledge, only a few studies have addressed this issue, and they all considered only the Mg end member (forsterite). In particular, two computational studies based on force-field calculations were performed on the main surfaces of forsterite,[12,13] whereas all of the other computational studies in the literature dealt with the adsorption of H, H_2, and H_2O on the (010) surface.[14−19]

In this article, we present a preliminary study to provide new insight into the structure and energetics of the crystal faces of forsterite, by means of ab initio quantum-mechanics calculations and a two-dimensional slab model. In particular, the equilibrium geometries and surface energies at 0 K of the (010), (101), (111), (001), (110), (120), and (021) faces of forsterite were determined. These results were then combined with experimental evidence to develop some considerations about the shape and genesis of olivine included in diamond, which displays, as we show herein, a crystal morphology that is very different from that of olivine crystals not entrapped inside diamond, as well as the equilibrium shape determined in this work. We propose an explanation accounting for these differences, by demonstrating that our results could provide crucial information on the diamond formation mechanism with respect to its guest inclusions, a topic that is still under strong debate in the scientific community.

Furthermore, as future computational works of our research group will be devoted to the study of the structure and energy of diamond/olivine interfaces (to study the epitaxial relationships between these phases and estimate the shape of olivine crystals included in diamond), the first step for such investigation is the assessment of our quantum-mechanical ab initio method in the description of clean olivine surfaces. Therefore, the present article can also be considered as an essential work to set the best computational parameters to use in ab initio calculations simulating diamond/olivine interfaces.

We employed a hybrid Hartree−Fock (HF)−density functional theory (DFT) approach that, notably, has never before been applied to the study of olivine surfaces. In particular, the B3LYP[20−22] functional was used, which has already demonstrated great accuracy in describing the surfaces of diamond,[23] as well as the structural, vibrational, and thermophysical properties of forsterite and fayalite.[24−28]

This article is structured as follows: Section 2 provides an outline of the computational methodology. In sections 3 and 4, the structures and energies of the surfaces are described and compared with the results of previous computational studies. Section 5 describes the application of the computational findings to the understanding of the shape and genesis of olivine included in diamonds, and the main conclusions are presented in section 6.

2. COMPUTATIONAL DETAILS

The calculations were performed at the DFT level with the periodic ab initio CRYSTAL09 code.[29−31] The hybrid B3LYP[20−22] Hamiltonian, already shown to provide accurate results for the structural and dynamical properties of olivine end members,[24−26,28] was employed. Crystal surfaces were simulated using a two-dimensional periodic slab model, consisting of a film formed by a set of atomic layers parallel to the *hkl* crystalline plane of interest.[32] The output files are freely available at http://mabruno.weebly/download.

In CRYSTAL, the multielectronic wave function is constructed as an antisymmetrized product (Slater determinant) of monoelectronic crystalline orbitals (COs) that are linear combinations of local functions (i.e., atomic orbitals, AOs) centered on each atom of the crystal. In turn, the AOs are linear combinations of Gaussian-type functions (GTFs, which are products of a Gaussian times a real solid spherical harmonic to give s-, p-, and d-type AOs). In this study, silicon, oxygen, and magnesium were described by (8s)−(6311sp)−(1d), (8s)−(411sp)−(1d), and (8s)−(511sp)−(1d) contractions, respectively. The exponents (in units of $bohr^{-2}$) of the most diffuse sp shells are 0.32 and 0.13 (Si), 0.59 and 0.25 (O), and 0.68 and 0.22 (Mg); the exponents of the single Gaussian d shell are 0.6 (Si), 0.5 (O), and 0.5 (Mg).[26,28]

The thresholds controlling the accuracy in the evaluation of Coulomb and exchange integrals (ITOL1, ITOL2, ITOL3, ITOL4, and ITOL5; see Dovesi et al.[29]) were set to 10^{-8} (ITOL1−ITOL4) and 10^{-16} (ITOL5). The threshold on the self-consistent-field (SCF) energy was set to 10^{-8} hartree.

In the employed package, the DFT exchange and correlation contributions are evaluated by numerically integrating functions of the electron density and of its gradient over the cell volume. The choice of the integration grid is based on an atomic partition method, originally developed by Becke.[33] In the present study, a pruned (75, 974) p grid was employed (XLGRID in the code[29]), which ensured a satisfactory accuracy in the numerically integrated electron charge density (the error was on the order of $1 \times 10^{-4}|e|$ of a total of $1120|e|$ for all considered surfaces).

The reciprocal space was sampled according to a Monkhorst−Pack mesh[34] with a shrinking factor of 4, corresponding to 10 *k* points in the first irreducible Brillouin zone.

Structures were optimized using the analytical energy gradients with respect to atomic coordinates and lattice parameters within a quasi-Newton scheme, combined with the Broyden−Fletcher−Goldfarb−Shanno scheme for Hessian updating.[35−37] Convergence was checked on energy, gradient components, and nuclear displacements. The threshold on energy between two subsequent optimization steps was set to 10^{-7} hartree; the thresholds on the root-mean square of the gradient components and nuclear displacements were set to 3.0×10^{-4} hartree $bohr^{-1}$ and 1.2×10^{-3} bohr, respectively; and the thresholds on the maximum components of the gradients and displacements were set to 4.5×10^{-4} hartree $bohr^{-1}$ and 1.8×10^{-3} bohr, respectively.

The specific surface energy γ (J/m^2) at a temperature of T = 0 K was calculated as[32]

$$\gamma = \lim_{n\to\infty} E_s(n) = \lim_{n\to\infty} \frac{E(n)_{slab} - nE_{bulk}}{2A} \quad (1)$$

where $E(n)$ is the energy of an *n*-layer slab, E_{bulk} is the energy of the bulk, A is the area of the surface unit cell, and the factor of 2 in the denominator accounts for the upper and lower surfaces of the slab model. $E_s(n)$ is thus the energy per unit area required for the formation of the surface from the bulk. As more layers are added in the calculation ($n \to \infty$), $E_s(n)$ converges to the surface energy per unit area (γ).

The number of d_{hkl} layers to be considered in each slab, *n*, was set to values such that the relative difference between $E_s(n)$ and $E_s(n-1)$ was <1%, to ensure a satisfactory convergence on surface energy and structure. In particular, within the computational scheme employed, *n* was set equal to 8, 4, 5,

dx.doi.org/10.1021/jp409837d | J. Phys. Chem. C 2014, 118, 2498−2506

8, 4, 4, and 4 for the (010), (101), (111), (001), (110), (120), and (021) surfaces, respectively, considered in this work (see Figures 1 and 2, as well as Figures S1−S5 of the Supporting Information). Then, the thicknesses of the converged (010), (101), (111), (001), (110), (120), and (021) slabs are $8d_{020}$ = 40.96, $4d_{101}$ = 14.96, $5d_{111}$ = 17.55, $8d_{002}$ = 23.92, $4d_{110}$ = 17.32, $4d_{120}$ = 14.00, and $4d_{021}$ = 15.56 Å, respectively; the optimized two-dimensional cell parameters of the slabs are listed in Table 1. All of these converged slabs were charge-neutral and contained 112 atoms; the center of inversion or a mirror plane parallel to the face was retained in the calculations, to ensure that the dipole moment perpendicular to the slab was equal to zero.

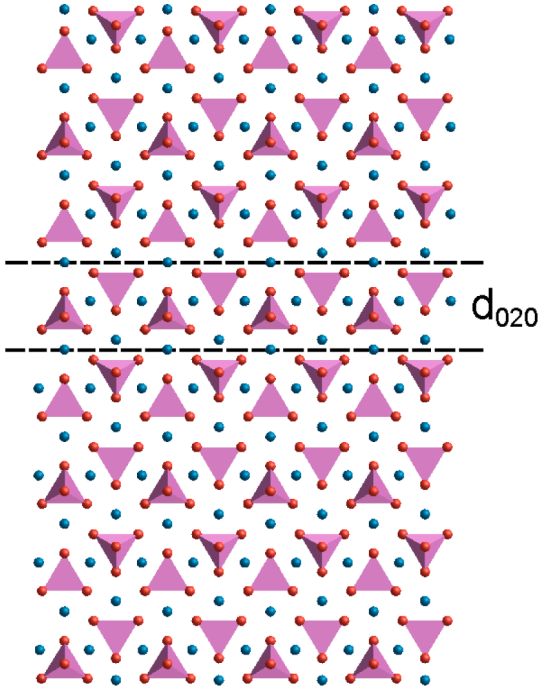

Figure 1. (010) surface viewed along [001]. d_{020} is the interplanar distance, i.e., the distance between adjacent 020 planes.

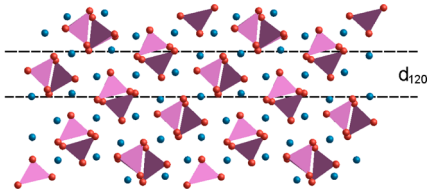

Figure 2. (120) surface viewed along [001]. d_{120} is the interplanar distance, i.e., the distance between adjacent 120 planes.

Table 1. Optimized Two-Dimensional Cell Parameters of the Seven Slabs under Study

	a (Å)	b (Å)	$\hat{a}b$ (deg)	area (Å^2)
(010)	4.7947	6.0432	90.00	28.97
(101)	7.7449	10.2534	90.11	79.41
(111)	7.6837	11.1473	105.08	82.70
(001)	4.8055	10.1488	91.03	48.76
(110)	6.1046	11.0616	90.00	67.53
(120)	6.0087	13.9318	90.40	83.71
(021)	4.8276	15.6504	89.66	75.55

3. STRUCTURE OF THE FORSTERITE SURFACES

The experimental bulk crystal structure (space group *Pbnm*; a_0 = 4.7490 Å, b_0 = 10.1985 Å, c_0= 5.9792 Å[38]) was allowed to relax within the employed computational scheme, giving a_0 = 4.7868 Å, b_0 = 10.2552 Å, and c_0 = 6.0108 Å. The crystal was then cut based on inspiration from 'T Hart,[39] who classified and studied the structures of the crystallographic forms of forsterite by applying the periodic bond chain (PBC) analysis of Hartman and Perdok.[40−42] According to this analysis, the (010), (101), (111), (001), (110), (120), and (021) faces are classified as *F* (flat) faces, having at least two PBCs running inside the slices with thickness d_{hkl}. Therefore, they are the most important faces in naturally occurring crystals.

Let us analyze the surface structural modifications in vacuo at T = 0 K by taking the ideal bulk structure as a reference. In particular, the distortion of the SiO_4 tetrahedral units belonging to the first layer of the slab, that is, the layer in contact with a vacuum, can be used as a quantitative measure of how much the surfaces reconstruct.

Table 2 reports the values of the Si−O bond distances for both the bulk and the seven surfaces analyzed. Notably, the first layer of the (010), (111), and (001) slabs was found to be made up of two independent tetrahedra, whereas in the case of the (101), (110), (120), and (021) slabs, four nonequivalent polyhedra were found. Two statistical indices can be employed to summarize the effects of atomic relaxation: the average Si−O bond distance per tetrahedron, ⟨Si−O⟩ (Å), and the difference between the maximum and minimum bond distances per tetrahedron, Δ (Å).

The average Si−O distance in forsterite is 1.6516 Å. Of the 22 symmetry-independent surface tetrahedra belonging to the seven slabs, 15 were found to have average distances lying within 0.01 Å of the bulk value. The seven average deviations from the bulk larger than 0.01 Å were found in the cases of (111) (both tetrahedra, 1.6684 and 1.6647 Å), (001) (1.6651 Å), (101) (1.6646 Å), (110) (two tetrahedra, 1.6793 and 1.6405 Å), and (120) (1.6667 Å). At the other extreme, all of the tetrahedra of both the (010) and (021) slabs were found to have average Si−O distances differing by only ±0.1% from the bulk value (absolute difference ≤ 0.003 Å).

The difference between the maximum and minimum Si−O distances in forsterite is 0.0446 Å. Only in two cases [0.0301 Å in (001), 0.0381 Å in (110)] was this deviation Δ found to be smaller in the slabs than in the bulk; in all other cases, it was larger, indicating the preference of tetrahedra at surfaces to increase their degree of distortion. The maximum Δ value was found in the case of (101), 0.1624 Å. The marked distortion of the tetrahedra was accompanied by large variations in the Mg−O distances and was due to a significant structural rearrangement suffered by the surfaces to increase their atomic density and reach a more stable configuration. Upon examination of the single Si−O distance values, we note that the longest Si−O distance (1.7376 Å) was observed for the (110) slab, whereas the shortest one (1.5679 Å) was found for the (101) slab.

The relaxed structures of the (010) and (120) surfaces (the most stable ones; see section 4) are shown in Figures 1 and 2; structures of the other five crystallographic orientations are reported in the Supporting Information.

Upon inspection of Figures 1, 2, and S1−S5 (Supporting Information) and the data reported in Table 2 and discussed in

dx.doi.org/10.1021/jp409837d | J. Phys. Chem. C 2014, 118, 2498−2506

Table 2. Optimized Si−O Distances (Å) of Forsterite and Its (010), (101), (111), (001), (110), (120), and (021) Surfaces at 0 K[a−c]

	bulk			(101)		
Si−O	1.6282		1.5940	1.5679	1.6261	1.6247
	1.6527		1.6232	1.6626	1.6453	1.6414
	1.6527		1.6878	1.6974	1.6560	1.6597
	1.6728		1.7079	1.7303	1.7061	1.6784
⟨Si−O⟩	1.6516		1.6532	1.6646	1.6584	1.6511
			+0.1	*+0.8*	*+0.4*	*0.0*
Δ	0.0446		0.1139	0.1624	0.0800	0.0537
			+155.4	*+264.1*	*+79.4*	*+20.4*
	(010)			(110)		
Si−O	1.6110	1.6272	1.5972	1.6438	1.6037	1.6131
	1.6437	1.6399	1.6971	1.6438	1.6037	1.6476
	1.6437	1.6399	1.7114	1.6716	1.6168	1.6476
	1.6967	1.7015	1.7114	1.6819	1.7376	1.6750
⟨Si−O⟩	1.6488	1.6521	1.6793	1.6603	1.6405	1.6458
	−0.2	*0.0*	*+1.7*	*+0.5*	*−0.7*	*−0.4*
Δ	0.0857	0.0743	0.1142	0.0381	0.1339	0.0619
	+92.2	*+66.6*	*+156.1*	*−14.6*	*+200.2*	*+38.8*
	(111)			(120)		
Si−O	1.6131	1.5877	1.5855	1.5916	1.6206	1.6373
	1.6622	1.6488	1.6513	1.6452	1.6526	1.6399
	1.6813	1.7099	1.7143	1.6615	1.6644	1.6549
	1.7170	1.7122	1.7156	1.6918	1.7058	1.7095
⟨Si−O⟩	1.6684	1.6647	1.6667	1.6475	1.6609	1.6604
	+1.0	*+0.8*	*+0.9*	*−0.2*	*+0.6*	*+0.5*
Δ	0.1039	0.1245	0.1301	0.1002	0.0852	0.0722
	+133.0	*+179.1*	*+191.7*	*+124.7*	*+91.0*	*+61.9*
	(001)			(021)		
Si−O	1.6179	1.6298	1.6053	1.6162	1.6112	1.6331
	1.6468	1.6362	1.6269	1.6428	1.6366	1.6392
	1.6684	1.6564	1.6625	1.6499	1.6501	1.6533
	1.7274	1.6599	1.7057	1.7054	1.7086	1.6895
⟨Si−O⟩	1.6651	1.6456	1.6501	1.6536	1.6516	1.6538
	+0.8	*−0.4*	*−0.1*	*+0.1*	*0.0*	*+0.1*
Δ	0.1095	0.0301	0.1004	0.0892	0.0974	0.0564
	+145.5	*−32.5*	*+125.1*	*+100.0*	*+118.4*	*+26.5*

[a]Surface data are reported for the SiO_4 tetrahedra lying on the first layer. Each column stands for a symmetry-independent tetrahedron: there are two in (010), (111), and (001) surfaces and four in the other surfaces. [b]⟨Si−O⟩ (Å) is the average Si−O bond length per tetrahedron; Δ (Å) is the difference between the maximum and minimum Si−O distance values. [c]Relative percentage differences of ⟨Si−O⟩ and Δ with respect to the bulk are reported in italics.

the previous paragraphs, it is worth noting that the face displaying the smallest surface relaxation was the (010) face. In this case, the first d_{020} layer suffered an extremely slight structural modification, as expected on the basis of experimental findings.[43] Furthermore, such a weak relaxation is associated with the lowest surface energy (see section 4).

4. SURFACE ENERGIES AND THE EQUILIBRIUM SHAPE AT 0 K OF FORSTERITE

Table 3 lists the surface energies γ of the seven crystallographic forms of forsterite analyzed in this work; they refer to the converged thick slabs discussed in section 2. The faces with the lowest and highest surface energies were found to be {010} and {110}, respectively. Then, the following stability order of the surfaces was obtained: (010) < (120) < (001) < (101) < (111) < (021) < (110).

Table 3. Surface Energies γ at 0 K (J/m^2) of the Main Crystal Faces of Forsterite and Percentage Variations Δ (%) with Respect to Previous Studies

face	this work	Watson et al.[13]	Δ (%)	de Leeuw et al.[12]	Δ (%)	Garcia-Gil et al.[14]	Δ (%)
(010)	1.22	1.28	−4.7	1.28	−4.7	1.20	1.7
(101)	1.78	1.81	−1.6	1.88	−5.3	–	–
(111)	1.84	1.80	2.2	1.81	1.6	–	–
(001)	1.78	1.61	10.1	1.74	2.3	–	–
(110)	2.18	2.28	−4.4	1.96	11.2	–	–
(120)	1.36	1.56	−12.8	1.56[a]	−12.8	–	–
(021)	1.90	1.95	−2.6	1.94	−2.1	–	–

[a]Calculated in this work using the force field of de Leeuw et al.[12]

As a comparison, Table 3 reports the surface energy values previously calculated by Watson et al.,[13] de Leeuw et al.,[12] and Garcia-Gil et al.;[14] because de Leeuw et al.[12] did not provide a surface energy for the (120) face, the value was calculated in this work by using their force field. There is good agreement between our values and those obtained at an empirical level by Watson et al.[13] and de Leeuw et al.[12] for the surfaces in a vacuum. Regarding the de Leeuw et al. values,[12] the highest difference (−12.8%) can be observed for the (120) face, whereas the lowest (1.6%) is related to the (111) face. In comparison, for the Watson et al. values,[13] the highest (−12.8%) and lowest (−1.6%) differences are related to the (120) and (101) faces, respectively. These results suggest that the force field employed by Watson et al.[13] and de Leeuw et al.[12] for describing atomic interactions in forsterite could be an effective starting point for studying the surfaces of this mineral.

Here, it is worth noting that Watson et al.[13] calculated the surface energies for three different terminations of the (110) face: (i) The surface termination with the highest surface energy (2.28 J/m^2) corresponds to the one considered in our work (2.18 J/m^2), whereas (ii) the surface termination with the lowest surface energy (1.70 J/m^2), which is the more stable surface termination, was not taken into account in our work. Therefore, for the sake of comparison with our data, in the following, we discuss only case i; however, it is important to stress that the more stable surface termination of the (110) face is that reported in the article by Watson et al.[13] Moreover, because of the very good agreement between our results and those from Watson et al.,[13] it is likely that the energy of the most stable (110) termination, if calculated by our approach, would be very similar to that reported by Watson et al.[13]

Finally, the work recently published by Garcia-Gil et al.[14] reported a (010) surface energy value (1.20 J/m^2) that is very close to the one estimated in the present study (1.22 J/m^2). This is not surprising, because these authors performed periodic first principles DFT calculations with the Perdew−Burke−Ernzerhof (PBE) functional.[25,44] Unfortunately, they studied the adsorption of H atoms on the (010) surface only; as a consequence, other crystal faces were disregarded.

By applying the Gibbs−Wulff theorem[45] and considering our surface energy values listed in Table 3, we were able to draw the equilibrium shape (ES) of a forsterite crystal in a vacuum at 0 K (Figure 3a). As a comparison, we also drew the ESs obtained using the surface energy values calculated by Watson et al.[13] (Figure 3b) and de Leeuw et al.[12] (Figure 3c).

dx.doi.org/10.1021/jp409837d | J. Phys. Chem. C 2014, 118, 2498−2506

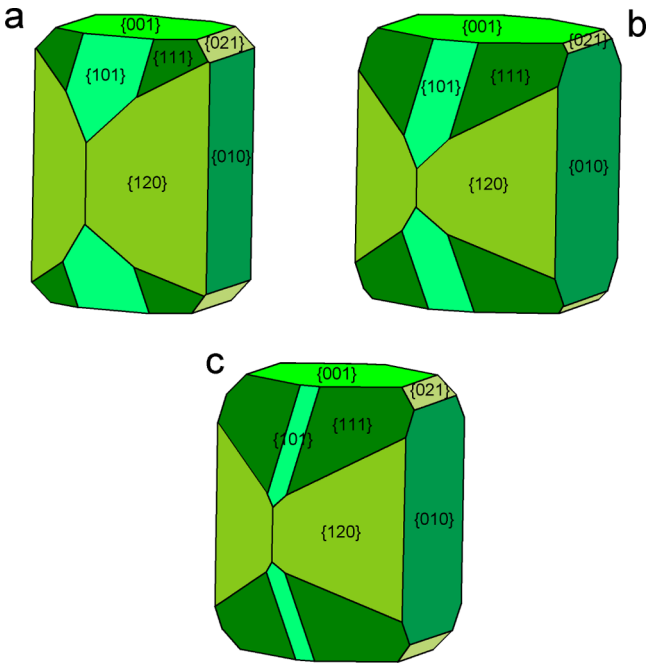

Figure 3. Equilibrium shapes (ESs) of forsterite at 0 K obtained with (a) surface energy values from this study, (b) surface energy values calculated by Watson et al.,[13] and (c) surface energies calculated by de Leeuw et al.[12]

To analyze quantitatively the differences occurring between the ES presented in this work and those published in previous studies, we computed the morphological relevance index (MRI) for all {*hkl*} forms; the MRI is defined as the percentage ratio between the total area of the faces belonging to a given {*hkl*} form and the total surface area of the crystal. The values are reported in Table 4. The morphological relevance order for

Table 4. Morphological Relevance Index (MRI) at 0 K (%) of the Main Crystal Faces of Forsterite and Absolute Variations Δ with Respect to Previous Studies

face	this work	Watson et al.[13]	Δ	de Leeuw et al.[12]	Δ
(010)	21.7	25.9	−4.2	24.9	−3.2
(101)	12.2	8.6	3.6	4.0	8.2
(111)	8.2	19.1	−10.9	25.6	−17.4
(001)	15.8	19.7	−3.9	16.2	−0.4
(110)	0.0	0.0	0.0	0.0	0.0
(120)	37.0	25.0	12.0	25.5[a]	11.5
(021)	5.1	1.7	3.4	3.8	1.3

[a]Calculated in this work by using the force field of de Leeuw et al.[12]

the ES proposed in this study (Figure 3a) is {120}, {010}, {001}, {101}, {111}, and {021}. A quite similar ES was obtained using Watson et al.'s data[13] (Figure 3b), with the following morphological relevance order: {010}, {120}, {001}, {111}, {101}, and {021}. The main difference is the inverted rankings of the {010} and {120} forms and of the {101} and {111} forms. Note that absolute differences between MRI values were as large as 12.0 in the case of (120); the smallest deviation was 3.4 for (021).

Finally, we considered the ES obtained by de Leeuw et al.[12] (Figure 3c), which was quite similar to the one determined in this work and had a morphological relevance order of {111}, {120}, {010}, {001}, {101}, and {021}. The main difference is the ranking of the {111} form, first instead of fifth. Only three of the forms had absolute deviations larger than 3.5: {111} with −17.4, {120} with 11.5, and {101} with 8.2.

Unfortunately, a comparison between theoretical and real ESs of olivine is not possible for the following two main reasons: (i) Olivine does not grow in a vacuum but is found in magmatic and metamorphic rocks. A correct evaluation of the ES requires knowledge of the free energies of the olivine/growth medium interfaces. (ii) The real morphologies are always obtained at $T > 0$ K, whereas our calculations were performed at $T = 0$ K. For a correct comparison between theoretical and real ESs, knowledge of how the temperature affects the interface free energy values, and hence the crystal ES, is fundamental. This implies the ability to calculate the vibrational and configurational entropy of the different olivine interfaces at the temperature of interest.

5. SOME CONSIDERATIONS ABOUT THE SHAPE AND GENESIS OF OLIVINE INCLUDED IN DIAMOND

The importance of studying the surfaces and shape of olivine is elucidated in this section, where it is shown how a detailed analysis of the crystal shape can reveal fundamental information for understanding the genesis of mineral inclusions in diamond. Indeed, the shape of olivine included in diamond is very different from that of olivine crystals not entrapped inside diamond, as well as from the equilibrium shape determined in this work. Therefore, in light of the results reported and discussed above, in this section, we try to explain such a morphological difference.

Diamond inclusions (DIs) are divided into three groups: protogenetic, syngenetic, and epigenetic.[46] DIs are classified as protogenetic when they form before encapsulation by the host diamond, whereas they are considered syngenetic when the inclusion and its host diamond form at the same time and by the same genetic processes. Both groups play a key role in the study of diamond formation processes, contrary to epigenetic phases, which are secondary minerals, usually associated with crustal processes, and are atypical with respect to the primary minerals in mantle xenoliths.

Such a distinction is important, because, in the case of syngenesis, any geological information extracted from the inclusion (e.g., pressure and temperature of formation, geochemical environment, age) would also unequivocally apply to its host diamond. On the other hand, a protogenetic inclusion would record conditions that existed before its encapsulation; the corresponding time range might span from short to very long geological time scales. In the latter case, the protogenetic inclusion could be completely unrelated to the formation of host diamond. Demonstrably protogenetic inclusions would support models of diamond formation involving fluxes of C-bearing fluids through pre-existing mantle rocks and could help explain occurrences of isotopically different inclusions in the same generation of diamond (e.g., Thomassot et al.[47]).

Distinguishing between syngenesis and protogenesis is as crucial as it is extremely difficult and controversial, as demonstrated by Taylor et al.[48] The most common observation used to deduce syngenesis is the imposition of the host diamond morphology on the DI (e.g., Meyer,[46,49] Pearson and Shirey,[50] Harris[51]). Concerning this argument, it is worth noting that the morphology of orthorhombic minerals (such as olivine and enstatite) included in diamond (with its well-known cubic symmetry) is usually described as "cuboctahedral".[11,48,52]

dx.doi.org/10.1021/jp409837d | J. Phys. Chem. C 2014, 118, 2498−2506

To explain such an "exotic" morphology, as reported by Taylor et al.,[48] a "... greater *form energy* of diamond (also named crystalloblastic force of diamond faces)" is invoked, "that thereby imposes its morphology upon the inclusion, during mutual growth". In the present study, we show that it is not necessary to resort to a rather undefined force to explain the shape of DIs; indeed, the observed morphology of olivine inclusions can be interpreted by means of only the crystallographic forms of the orthorhombic system, with no recourse to the crystallographic forms of the diamond cubic system.

Another significant contribution to the syngenesis-versus-protogenesis debate derives from the observation that some DIs occur in a specific orientational relationship with respect to diamond, which can be considered as evidence in favor of epitaxial growth of the DI above the diamond or vice versa and, hence, of syngenesis.[46,49,50,53−59] The first findings concerning possible epitaxial growth were those by Mitchell and Giardini,[59] who reported oriented inclusions of olivine in diamonds: the (010) face of olivine was parallel to the (111) face of diamond, and the [101] zone of olivine was parallel to the [101] zone of diamond. Wiggers de Vries et al.[60] recently reported electron-backscatter diffraction observations showing that the ⟨100⟩ crystallographic directions of diamond were parallel to the ⟨100⟩ directions of their chromite inclusions. In contrast, in a very recent work by our research group,[61] the crystallographic orientations of 47 olivines incorporated in 21 diamonds from Udachnaya kimberlite (Siberia) were analyzed, and at variance with the findings of Mitchell and Giardini,[59] no preferential orientation was observed between olivine and diamond. On this basis, a protogenetic origin was hypothesized for these olivines. In the present study, we discuss in more detail the mechanism of formation of DIs initially proposed by Nestola et al.[61] Such a mechanism is able to explain the somewhat different morphologies of olivine crystals included in diamond with respect to that of crystals outside the diamond host.

As pointed out above, the morphology of olivine included in diamond (i.e., orthorhombic against cubic symmetry) is usually described as cuboctahedral.[11,48,52] Indeed, the crystallographic forms of an orthorhombic mineral are pinacoid ({100}, {010}, and {001}), orthorhombic prism ({*hk*0}, {*h*0*l*}, and {0*kl*}), and orthorhombic bipyramid ({*hkl*}). Therefore, it is evident that the cube and octahedron cannot be used to properly describe the morphology of olivine; from a crystallographic point of view, referring to olivine morphology as cuboctahedral is wrong and can generate ambiguities in the process of interpreting the genesis of an inclusion.

Using an example, we now show that the so-called cuboctahedral shape of olivine inclusions is nothing more than a consequence of the association of orthorhombic forms. Figure 4 depicts a diamond showing the {100}-cube and {111}-octahedra forms, along with an olivine crystal having the pinacoids ({100}, {010}, and {001}) and the bipyramid {495}; the $a \equiv [100]$, $b \equiv [010]$, and $c \equiv [001]$ axes of olivine are parallel to the [100], [010], and [001] axes, respectively, of the diamond. Interestingly, the (495) face of olivine is a vicinal one, which ends up being parallel to the (111) face of the diamond; this can make it very difficult to distinguish olivine from diamond by observing only their morphologies: The shape of olivine might be equivalent to that of diamond, even if the forms making up the two crystals are completely different. The simple example reported here is meant to explain the origin of the ambiguities in describing the olivine morphology; it is worth stressing that, in other cases of mutual orientation

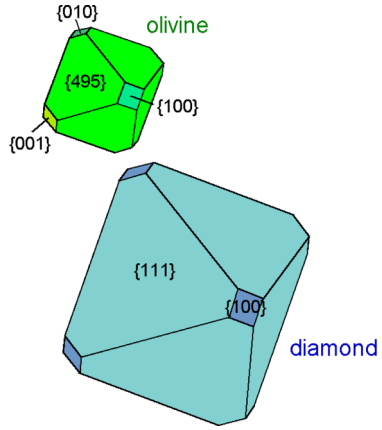

Figure 4. Diamond and olivine crystals showing the same shape but different crystallographic forms. The $a \equiv [100]$, $b \equiv [010]$, and $c \equiv [001]$ axes of olivine are parallel to the [100], [010], and [001] axes, respectively, of diamond.

between olivine and diamond, it is possible to identify a vicinal face of olivine having the same orientation as the (111) face of diamond.

In the following discussion, by taking into account our analysis of the olivine morphology and our previous study on the orientation of olivines included in diamonds from Udachnaya,[61] some considerations about the genesis of the DIs are reported.

As stated above, the most common observation used to deduce syngenesis is the imposition of the host diamond morphology on the DI (e.g., Meyer,[46,49] Pearson and Shirey,[50] Harris[51]). However, as demonstrated by Taylor et al.,[48] some peridotitic garnet inclusions (garnet is a silicate mineral, and peridotite is a rock composed mainly of olivine) having morphologies imposed by the host diamond clearly show a rare-earth element (REE) pattern typical of garnets found worldwide and not included in diamonds. Taylor et al.[48] stated that this observation is consistent with a protogenetic nature, at least for peridotitic garnets. Similar conclusions were drawn by Thomassot et al.,[47] who investigated isotopes of sulfide inclusions in diamonds, and Spetsius et al.,[62] who analyzed inclusions found in zircons extracted from diamonds.

To reconcile the geochemical observations on the REE pattern with the morphological observations, we propose the following mechanism for explaining the genesis of DIs; this mechanism, briefly described in the article by Nestola et al.,[61] is exemplified here by considering the formation of an olivine DI, but it can be easily generalized to DIs of any kind. Suppose that a diamond nucleates at time t_0 in a peridotitic rock (Figure 5), that is, when a C−H−O fluid becomes supersaturated with respect to the diamond phase. Then, the diamond grows and gains space at the expense of olivine, which dissolves at the diamond/olivine interface (Figure 5, time t_1). At a certain point in its growth history (Figure 5, time t_2), the diamond begins to include a piece of olivine, and at the same time, the diamond/olivine interface is adjusted through transport of matter by means of interface diffusion; in this way, the strain energy of the diamond/olivine interface is minimized, and the olivine morphology is modified. Finally, at time t_3 (Figure 5), the diamond fully envelops the olivine, which now has a completely different morphology than the external crystals; in parallel, the original geochemical fingerprint is left unchanged, as in the case of the peridotitic garnet inclusions described by Taylor et al.[48]

dx.doi.org/10.1021/jp409837d | J. Phys. Chem. C 2014, 118, 2498−2506

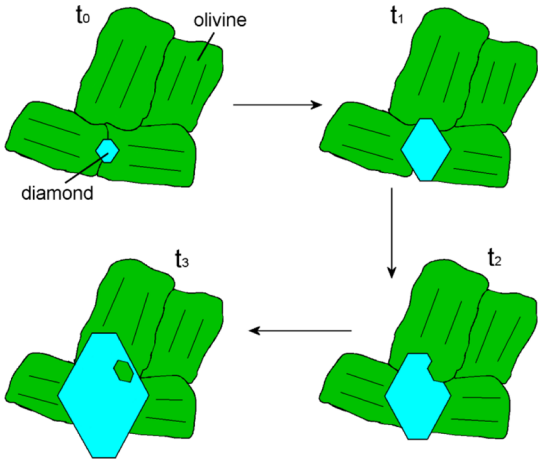

Figure 5. Schematic drawing representing the formation of an olivine inclusion in diamond.

As reported by Nestola et al.,[61] the result of the proposed mechanism is that, if the diamond growth is fast enough and the process temperature is not high enough to allow chemical and isotopic re-equilibration, then the DI might record age and $P-T$ conditions of formation that could be older than those of the host diamond.

Strong evidence in favor of this model is the finding of multiple inclusions of olivine within the same diamond showing similar orientations. Indeed, no more than three sets of iso-oriented olivines were found within a single diamond.[61] This could suggest that the probability of incorporating more than three original olivine monocrystals in a growing diamond is very low, and as a consequence, diamond should grow between adjacent grains of olivine.

Some interesting consequences derive from the proposed diamond growth mechanism:

(i) The morphology of a DI cannot be considered as evidence of syngenesis.
(ii) A DI preserves the original orientation of the crystal from which it is detached.
(iii) If the crystal morphology is modified but a DI does not show a preferential orientation with respect to the diamond (i.e., no epitaxial relationship between diamond and DI), then it is highly likely that the proposed growth mechanism is correct. This implies that the bulk of the DI is protogenetic, whereas its shape is syngenetic.
(iv) If the crystal morphology is modified and a DI shows a preferential orientation with respect to the diamond (i.e., epitaxial relationship between diamond and DI), then it is highly likely that the DI nucleated above a diamond face or vice versa. In this case, both the bulk and shape of the DI are syngenetic.

Up to now, we have discussed the case of a well-shaped DI, but the majority of DIs display rounded shapes, which is likely due to the development of a great number of vicinal faces during the process of diamond growth. In fact, some orientations of olivine are not able to produce the cuboctahedral-like shape discussed above. Then, to reduce the interface strain energy, the shape of olivine could adapt to diamond by realizing an envelope of vicinal faces that mimic a rounded morphology. Otherwise stated, in some cases, the olivine could have a crystallographic orientation that does not allow the development of a simple shape formed by a limited number of vicinal faces; a complex morphology composed of a large number of crystallographic forms would develop instead, to minimize the strain energy of the diamond/olivine interface. However, further studies are required to develop and validate this hypothesis. In particular, a detailed crystallographic analysis should be performed for determining the forms of the olivine included in diamond.

6. CONCLUSIONS

In this work, we have presented an accurate ab initio study of the structures and surface energies at 0 K of the low-index (010), (101), (111), (001), (110), (120), and (021) forsterite faces, by using for the first time, to the best of our knowledge, the hybrid Hartree–Fock/density functional B3LYP Hamiltonian and a localized all-electron Gaussian-type basis set. Furthermore, these results have been combined with experimental evidence to develop some considerations about the shape and genesis of olivine included in diamond, which show a crystal morphology very different from that of olivine crystals not entrapped inside diamond.

We can summarize our results as follows:

(i) The face displaying the smallest surface relaxation is the (010) face: The first d_{020} layer suffers an extremely slight structural modification, and as expected, such a weak relaxation is associated with the lowest surface energy value.
(ii) According to the surface energy values, the stability order of the forsterite faces is (010) < (120) < (001) < (101) < (111) < (021) < (110).
(iii) The equilibrium shape (ES) of a forsterite crystal was drawn by using our surface energy values. It was found to be quite similar to those determined at the empirical level by Watson et al.[13] and de Leeuw et al.[12] This suggests that the force field employed by those authors could be used as a starting point for fitting a new interatomic potential for studying the chemical reactions occurring at olivine/water interfaces.
(iv) As an example of the importance of understanding the surfaces and shape of olivine and a contribution to the syngenesis-versus-protogenesis debate, we discussed the peculiar crystal morphology of olivine included in diamond (DI). First, we showed that the observed cuboctahedral shape of olivine in diamond is actually a combination of an orthorhombic bipyramid (i.e., {495}) and pinacoids. This implies that the shape of olivine can be equivalent to that of diamond, even if the forms making up the two crystals are completely different. Second, we demonstrated that the morphology of the DI cannot be considered as evidence of syngenesis. In particular, if the crystal morphology is modified but the DI does not show a preferential orientation with respect to the diamond, the bulk of the DI is protogenetic, whereas its shape is syngenetic.

■ ASSOCIATED CONTENT

Supporting Information

Optimized structures of the (101), (111), (001), (110), and (021) faces of forsterite (Figures S1–S5). This material is available free of charge via the Internet at http://pubs.acs.org.

dx.doi.org/10.1021/jp409837d | J. Phys. Chem. C 2014, 118, 2498–2506

AUTHOR INFORMATION

Corresponding Author

*E-mail: marco.bruno@unito.it. Phone: (39) 0116705126. Fax: (39) 0116705128.

Notes

The authors declare no competing financial interest.

ACKNOWLEDGMENTS

F.N., M.B., and F.R.M. were supported by ERC Starting Grant 2012 (Grant 307322). R.D. acknowledges Curtin University for funding this research through the Curtin Research Fellowship scheme, iVEC@murdoch, and the Australian National Computational Infrastructure facilities for the provision of computer time. M.D.L.P. acknowledges Compagnia di San Paolo for financial support (Progetti di Ricerca di Ateneo-Compagnia di San Paolo-2011-Linea 1A, progetto ORTO11RRT5). Thanks are due to two anonymous reviewers for their careful reading of the manuscript and their fundamental observations on our work.

REFERENCES

(1) Dana, E. S. *A Textbook of Mineralogy*; Wiley: New York, 1941.

(2) Hiesinger, H.; Helbert, J. MERTIS Co-I Team, The Mercury Radiometer and Thermal Infrared Spectrometer (MERTIS) for the Bepi Colombo Mission. *Planet. Space Sci.* **2010**, *58*, 144−165.

(3) Antretter, M.; Fuller, M. Paleomagnetism and Rock Magnetism of Martian Meteorite ALH 84001. *Phys. Chem. Earth* **2002**, *27*, 1299−1303.

(4) Tarduno, J. A.; Cottrell, R. D.; Smirnov, A. V. The Paleomagnetism of Single Silicate Crystals: Recording Geomagnetic Feld Strength During Mixed Polarity Intervals, Superchrons, and Inner Core Growth. *Rev. Geophys.* **2006**, *41*, RG1002.

(5) Hwang, S. L.; Yui, T. F.; Chu, H. T.; Shen, P.; Iizuka, Y.; Yang, H. Y.; Yang, J.; Xu, Z. Hematite and Magnetite Precipitates in Olivine from the Sulu Peridotite: A Result of Dehyhrogenation-Oxidation Reaction of Mantle Olivine? *Am. Mineral.* **2008**, *93*, 1051−1060.

(6) Belley, F.; Ferré, E. C.; Martín-Hernández, F.; Jackson, M. J.; Dyar, M. D.; Catlos, E. J. The Magnetic Properties of Natural and Synthetic $(Fe_x, Mg_{1-x})_2$ SiO_4 Olivines. *Earth Planet. Sci. Lett.* **2009**, *284*, 516−526.

(7) Evans, B. W.; Hattori, K.; Baronnet, A. Serpentinite: What, Why, Where? *Elements* **2013**, *9*, 99−106.

(8) Power, I. M.; Wilson, S. A.; Dipple, G. M. Serpentinite Carbonation for CO_2 Sequestration. *Elements* **2013**, *9*, 115−121.

(9) McCollom, T. M.; Seewald, J. Serpentinites, Hydrogen, and Life. *Elements* **2013**, *9*, 129−134.

(10) Müntener, O. Serpentine and Serpentinization: A Link between Planet Formation and Life. *Geology* **2010**, *38*, 959−960.

(11) Stachel, T.; Harris, J. W. The Origin of Cratonic Diamonds—Constraints from Mineral Inclusions. *Ore Geol. Rev.* **2008**, *34*, 5−32.

(12) de Leeuw, N. H.; Parker, S. C.; Catlow, C. R. A.; Price, G. D. Modelling the Effect of Water on the Surface Structure and Stability of Forsterite. *Phys. Chem. Minerals* **2000**, *27*, 332−341.

(13) Watson, G. W.; Oliver, P. M.; Parker, S. C. Computer Simulation of the Structure and Stability of Forsterite Surfaces. *Phys. Chem. Miner.* **1997**, *25*, 70−78.

(14) Garcia-Gil, S.; Teillet-Billy, D.; Rougeau, N.; Sidis, V. H Atom Adsorption on a Silicate Surface: The (010) Surface of Forsterite. *J. Phys. Chem. C* **2013**, *117*, 12612−12621.

(15) Downing, C. A.; Ahmady, B.; Catlow, C. R. A.; de Leeuw, N. H. The interaction of hydrogen with the {010} surfaces of Mg and Fe olivine as models for interstellar dust grains: A density functional theory study. *Phil. Trans. R. Soc. A* **2013**, *371*, 20110592.

(16) King, H. E.; Stimpfl, M.; Deymier, P.; Drake, M. J.; Catlow, C. R. A.; Putnis, A.; de Leeuw, N. H. Computer Simulations of Water Interactions with Low-Coordinated Forsterite Surface Sites: Implications for the Origin of Water in the Inner Solar System. *Earth Planet. Sci. Lett.* **2010**, *300*, 11−18.

(17) Goumans, T. P. M.; Catlow, C. R. A.; Brown, W. A. Formation of H_2 on an Olivine Surface: A Computational Study. *Mon. Not. R. Astron. Soc.* **2009**, *393*, 1403−1407.

(18) Muralidharan, K.; Deymier, P.; Stimpfl, M.; de Leeuw, N. H.; Drake, M. J. Origin of Water in the Inner Solar System: A Kinetic Monte Carlo Study of Water Adsorption on Forsterite. *Icarus* **2008**, *198*, 400−407.

(19) de Leeuw, N. H. Density Functional Theory Calculations of Hydrogen-Containing Defects in Forsterite, Periclase, and α-Quartz. *J. Phys. Chem. B* **2001**, *105*, 9747−9754.

(20) Stephens, P. J.; Devlin, F. J.; Chabalowski, C. F.; Frisch, M. J. Ab Initio Calculation of Vibrational Absorption and Circular Dichroism Spectra Using Density Functional Force Fields. *J. Phys. Chem.* **1994**, *98*, 11623−11627.

(21) Becke, A. D. Density-Functional Thermochemistry. III. The Role of Exact Exchange. *J. Chem. Phys.* **1993**, *98*, 5648−5652.

(22) Lee, C.; Yang, W.; Parr, R. G. Development of the Colle−Salvetti Correlation Energy Formula into a Functional of the Electron Density. *Phys. Rev. B* **1988**, *37*, 785−789.

(23) De La Pierre, M.; Bruno, M.; Manfredotti, C.; Nestola, F.; Prencipe, M.; Manfredotti, C. The (100), (110) and (111) Surfaces of Diamond: An ab Initio B3LYP Study. *Mol. Phys.*, published online Sep 6, 2013, 10.1080/00268976.2013.829250.

(24) Noël, Y.; De La Pierre, M.; Maschio, L.; Rérat, M.; Zicovich-Wilson, C. M.; Dovesi, R. Electronic Structure, Dielectric Properties and Infrared Vibrational Spectrum of Fayalite: An Ab Initio Simulation with an All-Electron Gaussian Basis Set and the B3LYP Functional. *Int. J. Quantum Chem.* **2012**, *112*, 2098−2108.

(25) De La Pierre, M.; Orlando, R.; Maschio, L.; Doll, K.; Ugliengo, P.; Dovesi, R. Performance of Six Functionals (LDA, PBE, PBESOL, B3LYP, PBE0, and WC1LYP) in the Simulation of Vibrational and Dielectric Properties of Crystalline Compounds. The Case of Forsterite Mg_2SiO_4. *J. Comput. Chem.* **2011**, *32*, 1775−1784.

(26) Demichelis, R.; Civalleri, B.; Ferrabone, M.; Dovesi, R. On the Performance of Eleven DFT Functionals in the Description of the Vibrational Properties of Aluminosilicates. *Int. J. Quantum Chem.* **2010**, *110*, 406−415.

(27) Ottonello, G.; Civalleri, B.; Ganguly, J.; Vetuschi Zuccolini, M.; Noël, Y. Thermophysical Properties of the α−β−γ Polymorphs of Mg_2SiO_4: A Computational Study. *Phys. Chem. Miner.* **2009**, *36*, 87−106.

(28) Noël, Y.; Catti, M.; D'Arco, P.; Dovesi, R. The Vibrational Frequencies of Forsterite Mg_2SiO_4: An All-Electron Ab Initio Study with the CRYSTAL Code. *Phys. Chem. Miner.* **2006**, *33*, 383−393.

(29) Dovesi, R.; Saunders, V. R.; Roetti, C.; Orlando, R.; Zicovich-Wilson, C. M.; Pascale, F.; Civalleri, B.; Doll, K.; Harrison, N. M.; Bush, I. J.; D'Arco, Ph.; Llunell, M. *CRYSTAL09 User's Manual*; University of Torino: Torino, Italy, 2009.

(30) Dovesi, R.; Orlando, R.; Civalleri, B.; Roetti, C.; Saunders, V. R.; Zicovich-Wilson, C. M. CRYSTAL: A Computational Tool for the ab Initio Study of the Electronic Properties of Crystals. *Z. Kristallogr.* **2005**, *220*, 571−573.

(31) Pisani, C.; Dovesi, R.; Roetti, C. *Hartree−Fock Ab Initio Treatment of Crystalline Systems*; Lecture Notes in Chemistry; Springer: Berlin, 1988; Vol. *48*.

(32) Dovesi, R.; Civalleri, B.; Orlando, R.; Roetti, C.; Saunders, V. R. Ab Initio Quantum Simulation in Solid State Chemistry. In *Reviews in Computational Chemistry*; Lipkowitz, B. K., Larter, R., Cundari, T. R., Eds.; John Wiley & Sons, Inc.: New York, 2005; Vol. *21*, pp 1−125.

(33) Becke, A. D. Density-Functional Exchange-Energy Approximation with Correct Asymptotic Behavior. *Phys. Rev. A* **1988**, *38*, 3098−3100.

(34) Monkhrost, H. J.; Pack, J. D. Special Points for Brillouin-Zone Integration. *Phys. Rev. B* **1976**, *13*, 5188−5192.

(35) Civalleri, B.; D'Arco, Ph.; Orlando, R.; Saunders, V. R.; Dovesi, R. Hartree−Fock Geometry Optimisation of Periodic Systems with the CRYSTAL Code. *Chem. Phys. Lett.* **2001**, *348*, 131−138.

(36) Doll, K. Implementation of Analytical Hartree−Fock Gradients for Periodic Systems. *Comput. Phys. Commun.* **2001**, *137*, 74−88.
(37) Doll, K.; Saunders, V. R.; Harrison, N. M. Analytical Hartree−Fock Gradients for Periodic Systems. *Int. J. Quantum Chem.* **2001**, *82*, 1−13.
(38) Bostrom, D. Single-Crystal X-ray Diffraction Studies of Synthetic Ni−Mg Olivine Solid Solution. *Am. Mineral.* **1987**, *72*, 965−972.
(39) 'T Hart, J. The Structural Morphology of Olivine. I. A Qualitative Derivation. *Can. Mineral.* **1978**, *16*, 175−186.
(40) Hartman, P.; Perdok, W. G. On the Relations between Structure and Morphology of Crystals. I. *Acta Crystallogr.* **1955**, *8*, 49−52.
(41) Hartman, P.; Perdok, W. G. On the Relations between Structure and Morphology of Crystals. II. *Acta Crystallogr.* **1955**, *8*, 521−524.
(42) Hartman, P.; Perdok, W. G. On the Relations between Structure and Morphology of Crystals. III. *Acta Crystallogr.* **1955**, *8*, 525−529.
(43) Lemelle, L.; Abel, F.; Cohen, C.; Guyot, F. Study of the (010) Olivine Surface by Rutherford Backscattering Spectrometry in Channeling Geometry. *Am. Mineral.* **2002**, *87*, 327−332.
(44) Perdew, J. P.; Burke, K.; Ernzerhof, M. Generalized Gradient Approximation Made Simple. *Phys. Rev. Lett.* **1996**, *77*, 3865−3868.
(45) Wulff, G. Zur Frage der Geschwindigkeit des Wachstums und der Auflosung der Krystallflachen. *Z. Kristallogr. Kristallgeom.* **1901**, *34*, 949.
(46) Meyer, H. O. A. Inclusions in diamonds. In *Mantle Xenoliths*; Nixon, P. H., Ed.; John Wiley & Sons: Chichester, U.K., 1987; pp 501−522.
(47) Thomassot, E.; Cartigny, P.; Harris, J. W.; Lorand, J. P.; Rollion-Bard, C.; Chaussidon, M. Metasomatic Diamond Growth: A Multi-Isotope Study (^{13}C, ^{15}N, ^{33}S, ^{34}S) of Sulphide Inclusions and Their Host Diamonds from Jwaneng (Botswana). *Earth Planet. Sci. Lett.* **2009**, *282*, 79−90.
(48) Taylor, L. A.; Anand, M.; Promprated, P. Diamonds and Their Inclusions: Are the Criteria for Syngenesis Valid? *Proc. Int. Kimberlite Conf., 8th* **2003**, *1*, 1−5.
(49) Meyer, H. O. A. Genesis of Diamond: A Mantle Saga. *Am. Mineral.* **1985**, *70*, 344−355.
(50) Pearson, D. G.; Shirey, S. B. Isotopic dating of diamonds. In *Application of Radiogenic Isotopes to Ore Deposit Research and Exploration*; Reviews in Economic Geology; Lambert, D. D., Ruiz, J., Eds.; Society of Economic Geologists: Littleton, CO, 1999; pp 143−172.
(51) Harris, J. W. The Recognition of Diamond Inclusions. Part 1: Syngenetic Mineral Inclusions. *Ind. Diamond Rev.* **1968**, *28*, 402−410.
(52) Nestola, F.; Nimis, P.; Ziberna, L.; Longo, M.; Marzoli, A.; Harris, J. W.; Manghnani, M. H.; Fedortchouk, Y. First Crystal-Structure Determination of Olivine in Diamond: Composition and Implications for Provenance in the Earth's mantle. *Earth Planet. Sci. Lett.* **2011**, *305*, 249−255.
(53) Bulanova, G. P. The Formation of Diamond. *J. Geochem. Explor.* **1995**, *53*, 1−23.
(54) Leeder, O.; Thomas, R.; Klemm, W. *Einschlusse in Mineralien*; VEB Deutscher Verlag fur Grunstoffenindustrie: Leipzig, Germany, 1987.
(55) Harris, J. W.; Gurney, J. J. Inclusions in diamond. In *The Properties of Diamond*; Field, J. E., Ed.; Academic Press: London, 1979; pp 555−591.
(56) Sobolev, N. V. *Deep-Seated Inclusions in Kimberlites and the Problem of the Composition of the Upper Mantle*; American Geophysical Union: Washington, DC, 1977.
(57) Orlov, J. L. *The Mineralogy of Diamond*; Wiley: New York, 1977.
(58) Futergendler, S. I.; Frank-Kamenetsky, V. A. Oriented Inclusions of Olivine, Garnet and Chrome-Spinel in Diamonds. *Zap. Vses. Mineral. O-va.* **1961**, *90*, 230−236 (in Russian).
(59) Mitchell, R. S.; Giardini, A. A. Oriented Olivine Inclusions in Diamond. *Am. Mineral.* **1953**, *38*, 136−138.
(60) Wiggers de Vries, D. F.; Drury, M. R.; de Winter, D. A. M.; Bulanova, G. P.; Pearson, D. G.; Davies, G. R. Three-Dimensional Cathodoluminescence Imaging and Electron Backscatter Diffraction: Tools for Studying the Genetic Nature of Diamond Inclusions. *Contrib. Mineral. Petrol.* **2011**, *161*, 565−579.
(61) Nestola, F.; Nimis, P.; Angel, R. J.; Milani, S.; Bruno, M.; Prencipe, M.; Harris, J. W., manuscript in preparation.
(62) Spetsius, Z. V.; Belousova, E. A.; Griffin, W. L.; O'Reilly, S. Y.; Pearson, N. J. Archean Sulfide Inclusions in Paleozoic Zircon Megacrysts from the Mir kimberlite, Yakutia: Implications for the Dating of Diamonds. *Earth Planet. Sci. Lett.* **2002**, *199*, 111−126.